ROYAL SOCIETY OF CHEMISTRY

Nanoscale

Room-temperature surface-assisted reactivity of a melanin precursor: silver metal-organic coordination *versus* covalent dimerization on gold

Complete List of Authors:	De Marchi, Fabrizio; INRS, Univ. of Quebec,, Energy, Materials and Telecommunications Galeotti, Gianluca; INRS, Univ. of Quebec, Energy, Materials and Telecommunications Simenas, Mantas; Vilnius university, Faculty of Physics Tornau, Evaldas; Center for Physical Sciences and Technology,, Semiconductor Physics Institute Pezzella, Alessandro; Institute for Polymers, Composites and Biomaterials (IPCB); National Interuniversity Consortium of Materials Science and Technology (INSTM) MacLeod, Jennifer; Queensland University of Technology, School of Chemistry, Physics and Mechanical Engineering and Institute for Future Environments Ebrahimi, Maryam; INRS, Univ. of Quebec, Energy, Materials and Telecommunications Rosei, Federico; INRS, Energy, Materials and Telecommunications; University of Electronic Science and Technology of China, Institute for Fundamental and Frontier Science

SCHOLARONE™
Manuscripts

Nanoscale

ARTICLE

Room-temperature surface-assisted reactivity of a melanin precursor: silver metal-organic coordination *versus* covalent dimerization on gold

F. De Marchi,[a,†] G. Galeotti,[a,†] M. Simenas,[b] E. E. Tornau,[c] A. Pezzella,[d,e] J. MacLeod,[f,*] M. Ebrahimi,[a,$,*] F. Rosei[a,g,*]

The ability of catecholamines to undergo oxidative self-polymerization enables an attractive preparation route of coatings for biotechnology and biomedicine applications. However, efforts toward developing a complete understanding of the mechanism that underpins polymerization have been hindered by the multiple catechol crosslinking reaction pathways that occur during the reaction. Scanning tunneling microscopy allows the investigation of small molecules in a reduced-complexity environment, providing important insight into how the intermolecular forces drive the formation of supramolecular assemblies in a controlled setting. Capitalizing on this approach, we studied the self-assembly of 5,6 dihydroxy-indole (DHI) on Au(111) and Ag(111) to investigate the interactions that affect two-dimensional growth mechanism and to elucidate the behavior of the catechol group on these two surfaces. X-ray photoelectron spectroscopy, together with density functional theory and Monte Carlo modeling, help unravel the differences between the two systems. The molecules form large ordered domains, yet with completely different architectures. Our data reveal that some of the DHI molecules deposited on Ag are in a modified redox state, with their catechol group oxidized into quinone. On Ag(111), the molecules are disposed in long-range lamellar patterns stabilized by metal-organic coordination, while covalent dimer pairs are observed on Au(111). We also show that the oxidation susceptibility is affected by the substrate, with the DHI/Au remaining inert even after being exposed to O_2 gas.

Introduction

The development of efficient bottom-up approaches for the production of organic nanomaterials goes hand in hand with our progress in supramolecular chemistry, as we improve our understanding of the parameters that drive the self-organization of the small molecular building blocks into complex structures.[1]

The investigation of small model systems with limited functionalities is a crucial step,[2] as it allows to gain mechanistic insight on the molecular behaviour and learn how the intermolecular interactions affect the process,[3, 4] getting us closer to gain predictive control over this type of complex molecular assembly.

Molecular imaging done by scanning tunneling microscopy (STM) is often the starting point for the investigation of such systems.[5, 6] The ability to observe individual molecules at the atomic scale, along with the reduced complexity due to the presence of a substrate and the ultra-high vacuum (UHV) environment, makes STM an invaluable tool to explore the molecule-molecule and molecule-surface interactions.[7, 8]

Within this view, we continue our investigation over the self-assembled monolayer networks (SAMNs) of functionalized indoles[9] by presenting our work on 5,6-dihydroxyindole (DHI,[10] Figure 1a), in which a pyrrole ring is fused with a catechol.

Catechol (o-dihydroxybenzene) and its derivatives have gained increased attention in polymer chemistry in the past few years

a. Centre Energie, Materiaux et Telecommunications, Institut National de la Recherche Scientifique, 1650 Boulevard Lionel-Boulet, Varennes, QC, Canada J3X 1S2
b. Faculty of Physics, Vilnius University, Saulétekio 9. LT-10222 Vilnius, Lithuania
c. Semiconductor Physics Institute, Center for Physical Sciences and Technology, Saulétekio 3, LT-10222 Vilnius, Lithuania
d. Institute for Polymers, Composites and Biomaterials (IPCB), CNR, Via Campi Flegrei 34, I-80078 Pozzuoli (NA), Italy
e. National Interuniversity Consortium of Materials Science and Technology (INSTM), Florence 50121, Italy
f. School of Chemistry, Physics and Mechanical Engineering and Institute for Future Environments, Queensland University of Technology (QUT), 2 George Street, Brisbane, 4001 QLD, Australia
g. Institute for Fundamental and Frontier Science, University of Electronic Science and Technology of China, Chengdu 610054, PR China
† The authors contribute equally.
$ Current address: Physics Department E20, Technical University of Munich, James-Franck-Str.1, D-85748 Garching, Germany
* Corresponding authors' e-mail: jennifer.macleod@qut.edu.au, maryam.ebrahimi@emt.inrs.ca, rosei@emt.inrs.ca.
Electronic Supplementary Information (ESI) available: See DOI: 10.1039/x0xx00000x
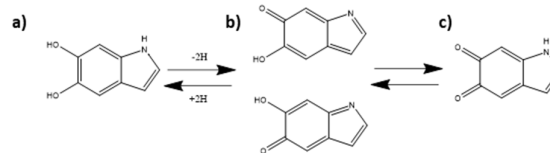
Figure 1: a) DHI and its oxidized forms b) indole semiquinone (SQ); c) indolequinone (IQ).

due to their versatile adhesiveness.[11, 12] In spite of that, the possible exploitation of catechol functional groups for applications in 2D self-assembly has not been investigated in detail, although their chemistry allows several interactions that would help the formation of stable nanostructures. While hydroxyl groups can create SAMNs stabilized by hydrogen bonding,[13-15] catechols can furthermore undergo reversible redox reactions, transforming into semiquinone and quinone forms (Figure 1); partial dehydrogenation can induce a phase transition to more robust architectures,[16-18] by exploiting the interactions between catechol and its oxidized forms.

The catechol-quinone pair reactivity is also behind the self-polymerization reactions of catecholamines,[19] of which the most prominent example is polydopamine.[20] While the reaction mechanism is still under debate, it is believed to involve the redox forms of catechol in a reverse dismutation reaction.[21] These ambiguities are reflected in the polydopamine's final structure, but it is commonly agreed that it consists of a supramolecular aggregate of different oligomers.[21]

DHI is also one of the last monomer intermediate products of the biochemical process that transforms tyrosine into melanin[22] - a promising material for bioelectronics applications.[20, 23, 24] Similar to polydopamine, the polymerization process and final structure of melanin are not yet completely understood,[25] however, it is known that different redox forms of DHI (Figure 1b-c) play an important role in the polymerization.[26]

The 111 facets of noble metals are chosen as the substrates since the interaction between the surface and the aromatic rings allows the molecule to adsorb in a planar geometry, with the molecules free to diffuse and form self-assembled networks. By comparing the results on the Ag(111) and Au(111) surface we gain insight on how the different surface reactivity affect the 2D growth.[27, 28]

Using STM we determine the structure of DHI SAMNs, while x-ray photoelectron spectroscopy (XPS) gives information on the chemical state of the molecule. Density functional theory (DFT) and Monte Carlo (MC) simulations are then used to corroborate the experimental hypothesis.

In this work, we present an investigation of the intermolecular interactions between catechol molecules as well as their reaction with the surface. We demonstrate that, along with intermolecular interactions, additional surface-mediated processes including catechol-quinone redox series of DHI play an essential role in the formation and structure of the SAMNs. On Au(111), our STM and Time-of-Flight Secondary Ion Mass Spectrometry (TOF-SIMS) data show the formation of DHI covalent dimers under ultra-high vacuum conditions at room temperature (RT).

Experimental

DHI was obtained commercially from Ark-pharm (95+% purity), and also synthesized (95+% purity) following the reaction of L-DOPA in a $K_3Fe(CN)_6$ and $NaHCO_3$ solution.[29] DHI was stored at -20 °C to avoid polymerization. All the experiments were

performed under UHV condition with a base pressure of 10^{-10} mbar. Both Ag(111) and Au(111) surfaces were cleaned by sequential sputtering (0.8 to 1.2 keV at 10^{-5} mbar of Ar for 15 minutes) and annealing (480 °C for 30 minutes) prior to deposition. DHI was deposited in a dedicated molecular beam epitaxy (MBE) chamber using an effusion (Knudsen) cell. To obtain monolayer coverage, the evaporator was kept at 60 °C for 15 minutes when dosing on Ag(111). To achieve a similar coverage on Au(111) it was necessary to keep the evaporator at 70 °C and deposit for 30 minutes. Samples were transferred between the preparation and analysis (MBE and STM) chambers through a load-lock transfer arm within the same UHV system. The STM images were recorded using a SPECS Aarhus 10 STM. All STM data were collected in constant-current mode. Bias voltages are reported with respect to the STM tip. Similar deposition conditions were applied to prepare the samples in a separate UHV chamber, followed by *in situ* XPS characterization with a SPHERA II U5 analyser from Scienta Omicron Gmbh, with Mg source (pass energy 20 eV and 1 second of dwell time).

To trigger oxidation, the same procedure was adopted in both UHV chambers: samples were exposed to O_2 gas by dosing through a leak valve in the main chamber, at a pressure of 10^{-6} mbar for 30 minutes.

All image processing and analysis were done using the free WSxM software.[30] Image calibrations were performed from STM images of the clean surface taken the same day and based on the known lattice constants of the substrates. More details on the lattice correction are described in the electronic supplementary information.

TOF-SIMS was carried out using a TOF-SIMS IV (IONTOF Gmbh) with a base pressure of 10^{-10} mbar. A 15 keV Bi^+ beam was used to sample an area of approximately $50 \times 50 \ \mu m^2$. Both positive and negative SIMS were performed at three different locations of the surface.

DFT calculations were performed with Vienna Ab-initio Simulation Package (VASP)[31, 32] using the Perdew-Burke-Ernzerhof[33] approximation (PBE) of the exchange-correlation potential, the projector augmented wave (PAW) method,[34, 35] and a plane-wave basis set with an energy cut-off of 450 eV. The dispersion forces were included in the calculations using DFT-D3 methods of Grimme.[36, 37] For the simulations of the reported SAMNs, gas phase calculations were performed in which all atoms were relaxed. All the calculations were performed at the gamma point until the net force on each atom was less than 0.02 eV/Å and the energy change between the two steps was smaller than 0.01 meV. The optimized structures are presented using VESTA software.[38]

Dimerization reaction energies were calculated under Gaussian09 software[39] by DFT using B3LYP hybrid functional approximation method with 6-311G(d,P) and 6-31G(d) basis set.

MC simulations[40] were performed on a square lattice of size $L \times L$ ($L = 96$) using Metropolis algorithm and Kawasaki dynamics. During the simulations, the number of molecules was fixed, and periodic boundary conditions were implemented. A randomly selected molecule was allowed to jump into an
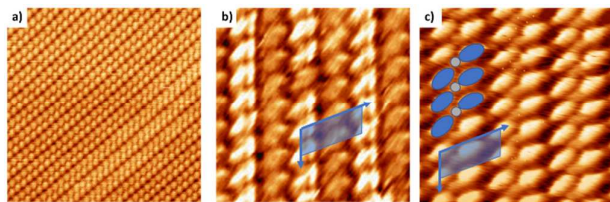
Figure 2: STM images of the as-deposited DHI/Ag(111) system; a) 20×20 nm² lamellar structures (0.23 nA, 0.51 V); 5×5 nm² of the lamellar phase taken at b) negative (-1.1 nA, -0.79 V) and c) positive (1 nA, 0.83 V) bias.

unoccupied lattice site. Such move was accepted with a probability exp(−ΔE/kT), where ΔE is the energy difference between the final (after the jump) and the initial (before the jump) state of the system. The Boltzmann constant is denoted as k. Up to 107 MC steps per site were performed to ensure a proper equilibration at each temperature. In the calculations, the thermodynamic temperature (T) and interaction energies are normalized by the strongest molecular interaction.

Results and Discussion

DHI on Ag(111)

After depositing DHI on Ag, the molecules assemble into lamellar structures across the surface (Figure 2a), which presents multiple orientation domains that extend up to hundreds of nanometres across the surface (Figure S1). Multi-domain STM images suggest the existence of six equivalent domains, reflecting the threefold symmetry of the substrate.

The lamellae are formed by molecular pairs whose dimensions suggests a non-covalently bonded assembly. The separation between the lamellae decreases as the molecular coverage increases (Figure S2), until reaching a close-packed structure with the unit cell dimension of u= 0.65 ± 0.05 nm, v= 1.65 ± 0.05 nm and angle of θ= 110 ± 2°. The contrast and shape of the molecules forming the dimer is not identical (Figure 2b). At positive bias an additional bright feature, likely a silver adatom, seems to be accommodated between the two molecules within the lamella (Figure 2c), which we tentatively assign as a metal-organic structure.[41, 42]

Although the STM images provide general insight into the molecular conformation on the surface, the specifics of the redox state of the molecule cannot be identified directly from the images. Furthermore, the molecule is prochiral, i.e., once deposited on the surface, two different isomers can be found,
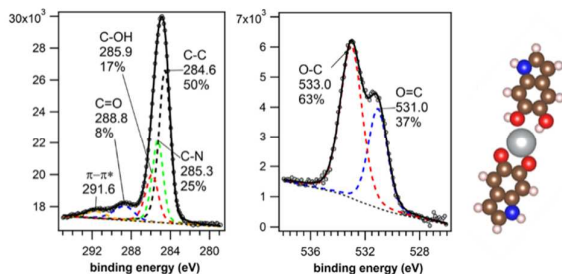
Figure 3: XPS spectra of the as-deposited DHI/Ag111 sample a) C 1s; b) O 1s; the components' peak position and overall ratio are reported; DFT model of the catechol-quinone metal-coordination dimer is shown in c).

increasing the number of possible molecular conformations. The contrast difference of these features may be due to having several conformations of DHI, due to its prochiral geometry, or to different oxidation states as the result of catechol-quinone redox. To properly characterize the lamellar structure, XPS measurement of the DHI molecular networks on Ag(111) was performed, described hereafter (Figure 3).

O 1s spectra reveal the presence of both catechol and quinone peaks at binding energies (BE) – whose peak position is in close agreement with values reported in the literature.[43, 44] The main peak at 533.0 eV (Figure 3b) is attributed to the hydroxyl group (O-C) of the catechol, while the peak at 2.0 eV lower BE (531.1 eV), is attributed to O=C, suggesting that some of the hydroxyl groups are oxidized to carbonyl. This is consistent with the corresponding C 1s spectra in which a peak at 288.7 eV, assigned to C=O, is identified (Figure 3a).[45] Analysis of the N 1s spectral region is challenging due to the proximity to the Ag 3d peak. Nevertheless, our fitting suggests a single peak at 400.0 eV, which can be related to C-N pyrrole[46, 47] (Figure S4). According to these data, we infer that DHI adsorbed on Ag(111) is present in two forms: the catechol and its oxidized counterpart as indole-5,6-quinone (IQ, Figure 1c). We can determine the proportion of the two redox forms from the 4:7 ratio between the area of the O=C (IQ) and O-C (DHI) components of the O 1s fit in Figure 3b.

Based on the STM and XPS result, we simulated by DFT calculations mixed catechol-quinone configurations, shown in Figure 3c and S6, including the surface in the simulation, in which the proposed metal-organic structure would represent a better geometry due to the interaction with surface atoms. In these models, the lamella is formed by a dimeric unit composed of one DHI and one IQ. A silver adatom is incorporated in the assembly, located between the quinone and the catechol. Based on the starting position of the hydrogen on the hydroxyl groups, the simulations converge towards the formation of a linear dimer (as shown in Figure S6a), or a more asymmetrical one (Figure 3c and S6d), with very similar energy (Δ=0.01 eV). In both of the cases, IQ is located closer to the substrate to maintain coordination with the Ag adatom, and the silver adatom lies closer to the oxygens of IQ than those of DHI. The DFT models suggest that the quinone strongly interacts with Ag adatoms, and the catechol hydroxyl groups further stabilize the assembly by forming hydrogen bonds between neighbouring O-H, C=O, and N-H groups. While both of the obtained DHI-Ag-IQ structure arrangements match the experimental data in term of dimensions, the asymmetric one better fits the molecular features and contrast of the STM image (as shown in Figure S8) While this model reproduces the features of the STM image, it does not match the ratio between DHI and IQ obtained from XPS. However, this disparity may be explained by the fact that XPS averages over a macroscopic area, and all smaller phases and defects (i.e. the pure DHI lamellae shown in figure S3) contribute to the quantification, affecting the ratio between the two redox species.

Annealing the surface did not produce any further oxidization nor the formation of a different self-assembly. The SAMNs are
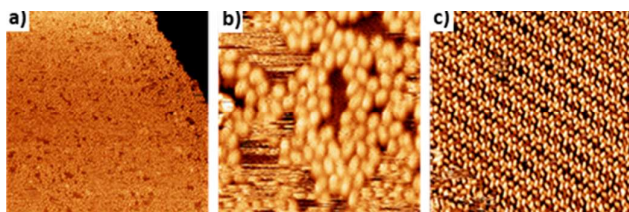
Figure 4: STM images of the DHI/Ag(111) after exposure to O₂ a) 45×45 nm² and (1.0 nA, 0.81 V) b) 7×7 nm² (0.1 nA, 0.32 V) c), 20×20 nm² mixed DHI and IQ ordered structure after O₂ exposure (0.1 nA, 0.24 V).

stable up to 250 °C, after which the molecules start to desorb from the surface. This result is in contrast with other reports in the literature,[17] where molecular moieties with hydroxyl groups show dehydrogenation already upon gentle annealing (< 100 °C).

Given our motivation to assess the catechol's reactivity on the surface, we attempted to trigger oxidation by exposing the 2D SAMNs on Ag(111) to oxygen.

Following oxygen exposure, our XPS spectra exhibit an obvious change in the O 1s peak (Figure 5c). An increase of the O=C peak at the expense of O-C was observed (Figure 5b). The FWHM of the O-C peak also strongly increased, which may be due to the multiple hydrogen bonding conformation adopted by the hydroxyl group.[48, 49] In addition, a third peak appears at 529.9 eV, which is related to the formation of silver oxide on the surface. When exposed to O₂, the bare surface of Ag forms only a small amount of AgO even after long exposure times. This is probably due to kinks and defects on the surface that are more prone to oxidation. On the other hand, once the molecule is on the surface, the quantity of formed Ag-O is much higher.

The transformation of catechol into quinone can also be deduced from the C 1s spectra (Figure 5a, Figure S5), where, in line with the O 1s data, there is an increase in the peak area assigned to C=O. The spectrum undergoes an overall shift of 0.2 eV towards lower BE, possibly due to the change in the work function of the Ag surface related to its partial oxidation as well as to the molecular rearrangement after the lamella disruption,[49, 50] and also shows an intensity loss due to molecular desorption.

From the morphological point of view, we see that the exposure to oxygen destroys the lamellar self-assembly, with the majority of the molecules assembled into disordered
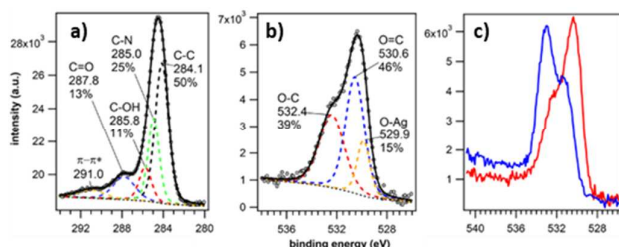
Figure 5: High resolution XPS spectra for the a) C 1s and b) O 1s components of DHI/Ag(111) exposed to O2 for 30 minutes. In addition, c) the comparison of the O 1s spectra before (blue) and after (red) O2 exposure; the components' peak position and overall ratio are reported.

clusters, as shown in Figure 4a and b. There is a lack of long-
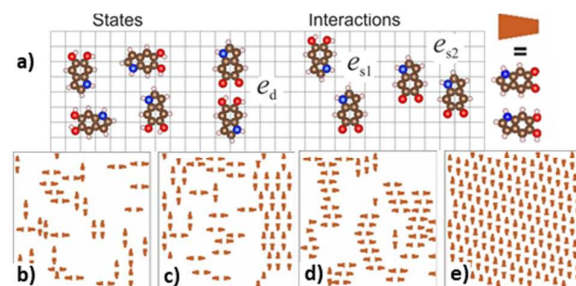
Figure 6: a) Four molecular states of DHI molecule and intermolecular interactions used for MC simulations. Snapshots of MC simulations obtained for b) es₁ = es₂ = 0, c) es₁ = 0.2, es₂ = 0, d) es₁ = 0, es₂ = 0.4 and e) es₁ = 0.2, es₂ = 0.4. Other simulation parameters: e_d = 1, T = 0.1. Experimentally observed lamellar structure is presented

range ordering and it is often possible to see small dots close to multiple molecules, suggesting that Ag adatoms are still incorporated in a metal-organic structure.

Small patches of ordered molecules with less than 50 nm² size were occasionally found on the surface, as shown Figure 4c, in which chains of alternating brighter molecules are disposed around a darker molecular moiety. This variation in STM contrast may be due to a different oxidation state of DHI, similar to what was shown in Figure 2b, or to a different disposition of the molecule with respect to its neighbours. The unit cell of this structure contains 14 molecules, and neither annealing nor further O₂ exposure led to larger ordered domains; for higher exposure (i.e. higher concentration of IQ) no ordered phase was

either witnessed. This is consistent with the work of Giovanelli et al.[16] where, after partial dehydrogenation, larger catechol containing molecules were able to reassemble in different ordered structures. Similar to the present report, further dehydrogenation did not improve the ordering, suggesting that a minimum catechol to quinone ratio was necessary for the stability of the structure.

We investigated the proposed ordered structures using MC simulations. Such calculations take entropic effects into account and help to identify the most important molecular interactions that are responsible for ordering.[51, 52] We obtained the experimental molecular arrangement using three interactions depicted in Figure 6. The main interaction is the catechol-quinone dimer (see the model shown in Figure 3c) characterized by energy e_d. We believe that this is the strongest interaction as the STM images mostly show chains of dimers and not of single molecules. The dimers are coupled together into chains with two side interactions es₁ and es₂ (Figure 6). We expect es₁ and es₂ to be significantly weaker than e_d. Interaction energies are kept as variable model parameters and normalized by the strongest catechol-quinone dimer interaction.

The snapshots of the MC simulations are presented in Figure 6 for different values of side interaction energies. The experimentally observed lamellar structure is obtained for a rather wide range of interaction parameters (es₁ < es₂ < e_d). Compared with other similar models,[53] a reasonable set of parameters is e_d = 1.0, es₁ = 0.2 and es₂ = 0.4 (see Figure 6e).
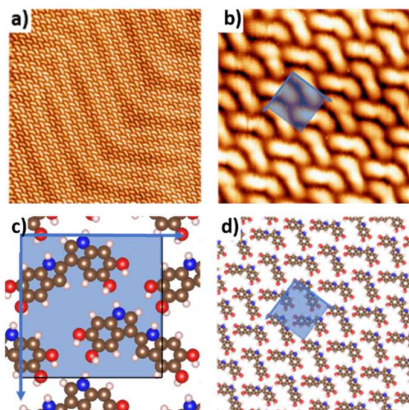
Figure 7: STM detail of the DHI/Au(111) a) 25×25 nm^2 (-0.1 nA, -0.83 V) b) 7×7 nm^2 (-1 nA, 0.14 V) c) and d) are simulated model for the banana-shape phase over the STM image of the DHI/Au(111) system.

Note that condition es$_1$ < es$_2$ is necessary to obtain the experimental phase. Otherwise, a less dense, higher symmetry structure, which is not observed in the experiment, is formed (see Figure S9). More details about the model and MC simulations are given in the supplementary material.

DHI on Au(111)

When deposited on Au, DHI molecules self-assemble in a structure different from the one observed on Ag(111). The unit cell is rectangular with the dimensions of u= 1.40 ± 0.1 nm, v= 1.53 ± 0.1 nm and θ= 90 ± 3° (Figure 7). Each cell contains a pair of banana-shape molecular dimers in a close-packed arrangement, disposed perpendicular to each other. The short length of these features (less than 1.3 nm) is not consistent with non-covalent assembly, thus we propose a covalent dimeric structure.

The XPS analysis of the DHI/Au(111) samples shows that the molecule is pure catechol. Although the O 1s peak is very close to the Au 4p peak, it is still evident by comparison with the spectrum of DHI/Ag(111) that only one component is present for DHI on Au(111). As additional confirmation, the C 1s (Figure 8a) does not show any peak related to a C=O component. The position of the C-C component is close to the one obtained for Ag, therefore discounts the presence of a C-Au organometallic bond, whose presence would be indicated by a component at a lower BE.[54] Again, the N 1s peak position is close to the
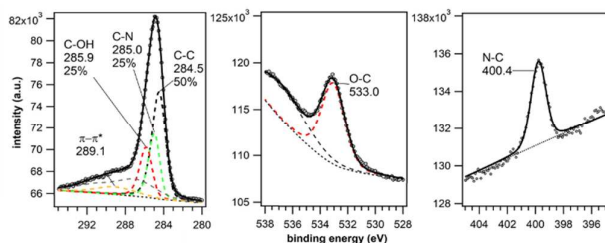
Figure 8: High resolution XPS spectra of the DHI/Au(111) a) C 1s, b) O 1s and c) N 1s; the components' peak position and overall ratio are reported. The XPS spectra of the Au sample before deposition is reported with a dashed grey line and has been taken in account during the fitting.

pyrrole one at 400.0 eV. The lack of an additional peaks at 399.0 eV related to the aromatic C=N-C bond excludes the presence of the semiquinone form.[55]

Similar to Ag, annealing does not affect molecular self-assembly on Au; however, unlike the Ag case, the molecular structures on Au remain unchanged following oxygen dosing, even after being exposed to atmospheric conditions.

Based on these experimental results, we hypothesize that the DHI/Au(111) system is composed of DHI-DHI covalently bonded dimers. While it is not unusual for molecules to polymerize on the Au surface, an annealing step is often required to trigger the polymerization.[56-58] To confirm that the structure observed by STM are DHI dimers, TOF-SIMS analysis of the sample was conducted (Figure 9). It is evident from the spectra that both the monomer and the dimer are present on the surface. TOF-SIMS also confirms different susceptibility to oxidation of the structures formed on the two studied substrates. On Au(111), no peak associated to IQ can be seen, thus confirming that the DHI/Au(111) remained stable during the transfer between the two UHV systems, without any oxidation process. An opposite result is obtained for Ag(111), where no dimer is visible, and the IQ peak is stronger than its reduced counterpart (Figure S10).

Although TOF-SIMS demonstrates the presence of dimerized DHI, the dimer geometry is not self-evident from STM. Different bonding conformations may lead to a planar dimer and a diversity of configurations had to be taken in account due to the prochirality of the molecule. These factors create the possibility for several regioisomers (presented in Figure S14). However, only one of the dimers, shown in Figure S14c, matches the dimensions and shape of the STM features, as it can be seen in Figure 7d.

These results show that the reaction of DHI on the (111) surfaces is strongly affected by the nature of the substrate itself. While on Ag the molecules react to form metal-organic structures, on Au they are instead able to bond with each other and form covalently bonded dimers.

The proposed covalent dimerization reaction on the surface has not been previously reported for 2D on-surface molecular study. Although DHI is well-known for its ability to polymerize under suitable conditions,[10, 25, 59] this is the first report presenting the polymerization of indole moieties, carried out under UHV at RT. On the other hand, while DHI oxidative polymerization usually leads to a range of products with different chain length and bonding motifs,[60] the presence of a surface constrains the process, producing only dimers that exhibit a bond at their 2-3 positions. The peculiar conformation of the dimers on the surface suggests that the dimerization is triggered by the indole ring reactivity. In an acidic environment, indole molecules may undergo a polymerization reaction that leads to their trimerization,[61] whose intermediate products are similar to the dimers shown in Figure 7c. On the other hand, since our STM and XPS analysis can only retrieve information on the already formed products, we have to account for the fact that different redox forms of DHI may be present during the dimerization process. This would allow for multiple possible reaction pathways and
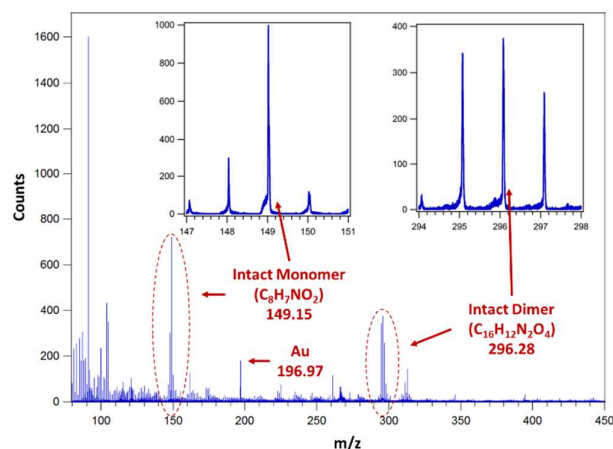
Figure 9: TOF-SIMS of the DHI/Au sample. The insets zoom over the area related to DHI monomer and dimers.

mechanisms (radical, ionic or even a combination of the two), such as SQ radical coupling[62] and DHI/IQ nucleophilic attack.[63] While being unable to discern between these different possibilities, we retrieved the reaction energy in the gas phase (reported in Table S3) and we find that the dimerization is energetically more favourable for SQ > IQ > DHI. The dimerization of the catechol form, in particular, is not thermodynamically favoured in the gas phase. In addition, our data shows that the same polymerization reaction does not occur on Ag(111). In contrast to the Au surface, the molecular structures imaged by STM do not indicate any dimer or polymer formation on Ag. The main difference between the two systems is in the redox state of the molecule. DHI is already partially oxidized into its IQ counterpart upon deposition on silver, and is further converted to IQ when exposed to O_2 gas. While a catechol group is not necessary to obtain the aforementioned acid polymerization,[64, 65] the oxidation in IQ enables new interactions that hinder the continuation of the polymerization process. As we have seen in our DFT data, IQ instead strongly interacts with the surface, bonding with adatoms and incorporating them into a self-assembled metal-organic network. This limits the diffusion of the molecule across the surface and prevents further reaction.

From the point of view of supramolecular chemistry, we have also seen that the presence of non-oxidized DHI molecules contributes to the formation of wide ordered domains, while after their conversion to IQ the molecules are arranged in disordered clusters. This inability to form long-range order may be due to the reduced diffusion of IQ molecules on the surface, hampered by metal-organic coordination, as well as the presence of silver oxide on the surface.

It was previously reported for catechol-containing molecules deposited on Ag[16-18] that similar dehydrogenation reactions can be thermally induced and used to create strong interactions between catechols and quinone. However, in our study, thermal annealing did not lead to dehydrogenation: no visible change in the structure was obtained until the desorption temperature was reached (200°C). This is probably

due to the lower adsorption energy of smaller molecules such as DHI, where the temperature of the dehydrogenation/oxidation process is higher than the desorption one. In contrast with what was previously reported, our data suggest that Ag adatoms might be incorporated in the networks, while the other studies have disregarded this possibility.[16, 17]

The possibility of achieving the same oxidation of the molecule on surface both thermally and by exposure to O_2 gas is promising, as it may open new reaction pathways for systems that do not tolerate thermal annealing. As we have seen in Figure 4c, variations in the IQ/DHI ratio may drive the system towards the formation of a different self-assembled architecture. With a judicious choice of molecule and surface, this on-surface oxidation may be triggered and better controlled, as well as used as a tool for engineering of the chemistry and topology of biologically-relevant molecular layers at surfaces.

Conclusions

We have reported our investigation of the self-assembly of DHI over the (111) surfaces of Ag and Au. When deposited on Ag(111), the molecule partially oxidizes upon adsorption, forming long-range ordered metal-organic structures composed of a mixture of catechols and quinones. Further exposure to oxygen leads to additional conversion of the catechol species into quinone. Oxygen exposure causes an increase in IQ and can trigger a phase transition of the SAMNs, however a full layer of IQ does not create structures with long-range order.

On Au(111), DHI bonds into covalent dimers, and does not undergo further oxidation, even if exposed to O_2. The exposure does not lead to any morphological or chemical change in the molecule. The size of the imaged features in STM does not match with single molecule but suggests a covalent dimer structures which is consistent with species present in TOF-SIMS measurements of the surface. The dimer shape and dimension suggest that a mechanism similar to indole polymerization in acid solution is involved. However, unlike the solution case, a cyclic trimer was not obtained.

Our study demonstrates that the UHV STM is a convenient approach for the investigation of the multiple chemical reactions that lead to the catecholamine polymerization. The reduced complexity environment helps us better understand how the molecule-surface interactions strongly affect the catechol group, driving the formation of different 2D structures with different chemical bondings. By investigating other eumelanin precursors, we may be able to gain important insight on the pigment complex structure, as well as understand the differences with other synthetic eumelanin-like polymers preparation routes.

Furthermore, our study revealed an interesting coupling reaction that leads to the DHI dimerization o Au. This may be exploited for the preparation of 2D conjugated polymers, but further investigation is required, to better clarify the

mechanism of the reaction and the role of the catechol group in the process.

Conflicts of interest

There are no conflicts to declare.

Acknowledgements

Notes and references

1. G. M. Whitesides and M. Boncheva, *Proc. Natl. Acad. Sci.*, 2002, **99**, 4769-4774.
2. C. Heininger, L. Kampschulte, W. A. Heckl and M. Lackinger, *Langmuir*, 2009, **25**, 968-972.
3. J.-M. Lehn, *Proc. Natl. Acad. Sci.*, 2002, **99**, 4763-4768.
4. F. Rosei, M. Schunack, Y. Naitoh, P. Jiang, A. Gourdon, E. Laegsgaard, I. Stensgaard, C. Joachim and F. Besenbacher, *Prog. Surf. Sci*, 2003, **71**, 95-146.
5. J. V. Barth, *Annu. Rev. Phys. Chem*, 2007, **58**, 375-407.
6. J. K. Gimzewski and C. Joachim, *Science*, 1999, **283**, 1683-1688.
7. R. Otero, J. M. Gallego, A. L. V. de Parga, N. Martín and R. Miranda, *Adv. Mater*, 2011, **23**, 5148-5176.
8. R. Otero, W. Xu, M. Lukas, R. E. A. Kelly, E. Lægsgaard, I. Stensgaard, J. Kjems, L. N. Kantorovich and F. Besenbacher, *Angew. Chem*, 2008, **120**, 9819-9822.
9. F. De Marchi, D. Cui, J. Lipton-Duffin, C. Santato, J. M. MacLeod and F. Rosei, *J. Chem. Phys*, 2015, **142**, 101923.
10. M. D'Ischia, A. Napolitano, A. Pezzella, E. J. Land, C. A. Ramsden and P. A. Riley, in *Advances in Heterocyclic Chemistry*, ed. R. K. Alan, Academic Press, 2005, vol. Volume 89, pp. 1-63.
11. Q. Ye, F. Zhou and W. Liu, *Chem. Soc. Rev*, 2011, **40**, 4244-4258.
12. E. Faure, C. Falentin-Daudré, C. Jérôme, J. Lyskawa, D. Fournier, P. Woisel and C. Detrembleur, *Prog. Polym. Sci*, 2013, **38**, 236-270.
13. A. C. Marele, I. Corral, P. Sanz, R. Mas-Ballesté, F. Zamora, M. Yáñez and J. M. Gómez-Rodríguez, *J. Phys. Chem. C*, 2013, **117**, 4680-4690.
14. H.-M. Zhang, J.-W. Yan, Z.-X. Xie, B.-W. Mao and X. Xu, *Chem. Eur. J*, 2006, **12**, 4006-4013.
15. S. Buchholz and J. P. Rabe, *Angew. Chem. Int. Ed*, 1992, **31**, 189-191.
16. L. Giovanelli, O. Ourdjini, M. Abel, R. Pawlak, J. Fujii, L. Porte, J.-M. Themlin and S. Clair, *J. Phys. Chem. C*, 2014, **118**, 14899-14904.
17. R. Pawlak, S. Clair, V. Oison, M. Abel, O. Ourdjini, N. A. A. Zwaneveld, D. Gigmes, D. Bertin, L. Nony and L. Porte, *ChemPhysChem*, 2009, **10**, 1032-1035.
18. S. Clair, S. Pons, A. P. Seitsonen, H. Brune, K. Kern and J. V. Barth, *J. Phys. Chem. B*, 2004, **108**, 14585-14590.
19. D. G. Graham, *Mol. Pharmacol*, 1978, **14**, 633-643.
20. Y. Liu, K. Ai and L. Lu, *Chem. Rev*, 2014, **114**, 5057-5115.
21. J. Yang, M. A. Cohen Stuart and M. Kamperman, *Chem. Soc. Rev*, 2014, **43**, 8271-8298.
22. S. Hong, Y. S. Na, S. Choi, I. T. Song, W. Y. Kim and H. Lee, *Adv. Funct. Mater*, 2012, **22**, 4711-4717.
23. M. Ambrico, P. F. Ambrico, T. Ligonzo, A. Cardone, S. R. Cicco, M. D'Ischia and G. M. Farinola, *J. Mater. Chem. B*, 2015, **3**, 6413-6423.
24. J. Wünsche, L. Cardenas, F. Rosei, F. Cicoira, R. Gauvin, C. F. O. Graeff, S. Poulin, A. Pezzella and C. Santato, *Adv. Funct. Mater*, 2013, **23**, 5591-5598.
25. S. J. Orlow, M. P. Osber and J. M. Pawelek, *Pigment Cell Melanoma Res*, 1992, **5**, 113-121.
26. M. D'Ischia, K. Wakamatsu, A. Napolitano, S. Briganti, J. C. Garcia-Borron, D. Kovacs, P. Meredith, A. Pezzella, M. Picardo, T. Sarna, J. D. Simon and S. Ito, *Pigment Cell Melanoma Res*, 2013, **26**, 616-633.
27. J. Björk, F. Hanke and S. Stafström, *J. Am. Chem. Soc*, 2013, **135**, 5768-5775.
28. J. Björk, Y.-Q. Zhang, F. Klappenberger, J. V. Barth and S. Stafström, *J. Phys. Chem. C*, 2014, **118**, 3181-3187.
29. A. Corani, A. Huijser, T. Gustavsson, D. Markovitsi, P.-Å. Malmqvist, A. Pezzella, M. D'Ischia and V. Sundström, *J. Am. Chem. Soc*, 2014, **136**, 11626-11635.
30. I. Horcas, R. Fernandez, J. M. Gomez-Rodriguez, J. Colchero, J. Gomez-Herrero and A. M. Baro, *Rev. Sci. Instrum*, 2007, **78**.
31. G. Kresse and J. Hafner, *Phys. Rev. B*, 1993, **47**, 558-561.
32. G. Kresse and J. Furthmüller, *Phys. Rev. B*, 1996, **54**, 11169-11186.
33. J. P. Perdew, M. Ernzerhof and K. Burke, *J. Chem. Phys.*, 1996, **105**, 9982-9985.
34. P. E. Blöchl, *Phys. Rev. B*, 1994, **50**, 17953-17979.
35. G. Kresse and D. Joubert, *Phys. Rev. B*, 1999, **59**, 1758-1775.
36. S. Grimme, J. Antony, S. Ehrlich and H. Krieg, *J. Chem. Phys.*, 2010, **132**, 154104.
37. S. Grimme, *J. Comput. Chem.*, 2006, **27**, 1787-1799.
38. K. Momma and F. Izumi, *J. Appl. Crystallogr*, 2011, **44**, 1272-1276.

39. Frisch, M.; Trucks, G.; Schlegel, H. B.; Scuseria, G.; Robb, M.; Cheeseman, J.; Scalmani, G.; Barone, V.; Mennucci, B.; Petersson, G., Gaussian 09, revision a. 02, gaussian. *Inc., Wallingford, CT* **2009,** *200*.

40. D. Landau and K. Binder, *A Guide to Monte Carlo Simulations in Statistical Physics*, Cambridge University Press, 2005.

41. S. Stepanow, N. Lin, D. Payer, U. Schlickum, F. Klappenberger, G. Zoppellaro, M. Ruben, H. Brune, J. V. Barth and K. Kern, *Angew. Chem*, 2007, **119**, 724-727.

42. A. C. Papageorgiou, J. Li, S. C. Oh, B. Zhang, O. Saglam, Y. Guo, J. Reichert, A. B. Marco, D. Cortizo-Lacalle, A. Mateo-Alonso and J. V. Barth, *Nanoscale*, 2018, DOI: 10.1039/C8NR02537A.

43. F. Bebensee, K. Svane, C. Bombis, F. Masini, S. Klyatskaya, F. Besenbacher, M. Ruben, B. Hammer and T. Linderoth, *Chem. Comm*, 2013, **49**, 9308-9310.

44. B. Yang, J. Björk, H. Lin, X. Zhang, H. Zhang, Y. Li, J. Fan, Q. Li and L. Chi, *J. Am. Chem. Soc*, 2015, **137**, 4904-4907.

45. S. Yumitori, *Journal of Materials Science*, 2000, **35**, 139-146.

46. G. Beamson and D. Briggs, *High Resolution XPS of Organic Polymers: The Scienta ESCA300 Database*, Wiley, 1992.

47. R. J. J. Jansen and H. van Bekkum, *Carbon*, 1995, **33**, 1021-1027.

48. S. Garcia-Gil, A. Arnau and A. Garcia-Lekue, *Surf. Sci*, 2013, **613**, 102-107.

49. M. Chen, J. Xiao, H.-P. Steinrück, S. Wang, W. Wang, N. Lin, W. Hieringer and J. M. Gottfried, *J. Phys. Chem. C*, 2014, **118**, 6820-6830.

50. D. A. Hutt and C. Liu, *Appl. Surf. Sci*, 2005, **252**, 400-411.

51. M. Šimėnas and E. E. Tornau, *J. Chem. Phys*, 2013, **139**, 154711.

52. S. J. Stoneburner, V. Livermore, M. E. McGreal, D. Yu, K. D. Vogiatzis, R. Q. Snurr and L. Gagliardi, *J. Phys. Chem. C*, 2017, **121**, 10463-10469.

53. A. Ibenskas, M. Šimėnas and E. E. Tornau, *J. Phys. Chem. C*, 2018, **122**, 7344-7352.

54. A. Basagni, L. Ferrighi, M. Cattelan, L. Nicolas, K. Handrup, L. Vaghi, A. Papagni, F. Sedona, C. D. Valentin, S. Agnoli and M. Sambi, *Chem. Comm*, 2015, **51**, 12593-12596.

55. L. Jiang, A. C. Papageorgiou, S. C. Oh, Ö. Sağlam, J. Reichert, D. A. Duncan, Y.-Q. Zhang, F. Klappenberger, Y. Guo, F. Allegretti, S. More, R. Bhosale, A. Mateo-Alonso and J. V. Barth, *ACS Nano*, 2016, **10**, 1033-1041.

56. Q. Li, B. Yang, H. Lin, N. Aghdassi, K. Miao, J. Zhang, H. Zhang, Y. Li, S. Duhm, J. Fan and L. Chi, *J. Am. Chem. Soc*, 2016, **138**, 2809-2814.

57. L. Lafferentz, V. Eberhardt, C. Dri, C. Africh, G. Comelli, F. Esch, S. Hecht and L. Grill, *Nat. Chem*, 2012, **4**, 215.

58. D. Zhong, J.-H. Franke, S. K. Podiyanachari, T. Blömker, H. Zhang, G. Kehr, G. Erker, H. Fuchs and L. Chi, *Science*, 2011, **334**, 213-216.

59. D. Billaud, E. B. Maarouf and E. Hannecart, *Synth. Met*, 1995, **69**, 571-572.

60. A. Pezzella, A. Napolitano, M. D'Ischia and G. Prota, *Tetrahedron*, 1996, **52**, 7913-7920.

61. L. Panzella, A. Pezzella, M. Arzillo, P. Manini, A. Napolitano and M. D'Ischia, *Tetrahedron*, 2009, **65**, 2032-2036.

62. A. Pezzella, O. Crescenzi, L. Panzella, A. Napolitano, E. J. Land, V. Barone and M. d'Ischia, *J. Am. Chem. Soc*, 2013, **135**, 12142-12149.

63. H. Okuda, K. Wakamatsu, S. Ito and T. Sota, *J. Phys. Chem. A*, 2008, **112**, 11213-11222.

64. P. Manini, V. Criscuolo, L. Ricciotti, A. Pezzella, M. Barra, A. Cassinese, O. Crescenzi, M. G. Maglione, P. Tassini, C. Minarini, V. Barone and M. D'Ischia, *ChemPlusChem*, 2015, **80**, 919-927.

65. X.-C. Li, C.-Y. Wang, W.-Y. Lai and W. Huang, *J. Mater. Chem. B*, 2016, **4**, 10574-10587.
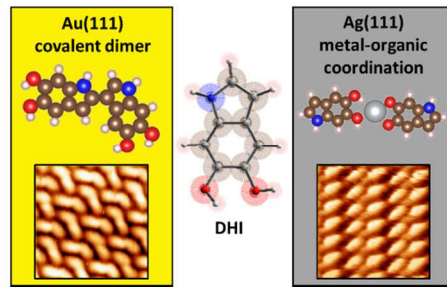
Surface drives self-assembly of a cathecol-indole molecule - triggering metal-organic coordination on silver and dimerization on gold at room temperature.